DR MARIO CACCIA (Orcid ID : 0000-0003-0190-5111)

Article type : Article

Associate Editor: Professor Katherine Faber

Synthesis of high-surface area mesoporous SiC with hierarchical porosity for use as catalyst support

A. Ortega-Trigueros[1], J. Narciso[1,2], M. Caccia[3,*]

[1] Instituto Universitario de Materiales (IUMA) University of Alicante, Alicante, Spain

[2]Centre for Materials Science and Nanotechnology, Department of Chemistry, University of Oslo, Oslo, Norway

[3] Materials Engineering Department, Purdue University, West Lafayette, IN, USA

[*]Corresponding author: mariorcaccia@gmail.com

Abstract:

Porous SiC with a hierarchical mesoporous structure is a promising material for high-performance catalytic systems because of its high thermal conductivity, high chemical inertness at high temperature and oxidation resistance. Attempts to produce high-surface area hierarchical SiC have typically been made by using a porous carbon as a template and reacting it with either Si or SiO_2 at high temperature under inert atmosphere. Because the reaction mechanism with Si involves a carbon dissolution step, and the reaction with SiO_2 is highly dependent on C-SiO_2 dispersion, the porous structure of the carbon template is not maintained, and the reaction yields non-porous SiC. In this work, mesoporous SiC has been synthesized using a novel hard-template methodology. SiC was prepared from a hierarchical (mesoporous) silica which served as a solid template. Carbon deposition was done by Carbon Vapor Deposition (CVD) using CH_4 as carbon precursor, where different temperatures and reaction times were tested to optimize the carbon

This article has been accepted for publication and undergone full peer review but has not been through the copyediting, typesetting, pagination and proofreading process, which may lead to differences between this version and the Version of Record. Please cite this article as doi: 10.1111/JACE.17285

coating. The synthesized SiC retained 61 (118 m^2/g) and 47% (0.3 cm^3/g) of the BET surface area and the mesopore volume of the original SiO_2, which is 10 times higher than the retention reported for other template methods used to produce high surface area SiC.

Keywords: SiC, mesoporous material

1. Introduction

Catalyst supports are typically oxide or carbon-based materials due to their high thermal and chemical stability. Although the use of these materials is widespread, they present certain disadvantages. Oxides like alumina (Al_2O_3) and silica (SiO_2) have low thermal conductivity and a certain chemical reactivity that produces loss of the active phase (metals) in a catalyst [1–4]. Carbon materials present mainly two issues; in the first place they exhibit low resistance to oxidation which limits them to reactions that require an inert atmosphere; and on the other hand the existence of micropores that limit the mass transfer of the reactants due to diffusional problems [5,6]. In this context, there is a great interest for developing and synthesizing new materials that can act as catalyst supports with enhanced performance compared to oxides or carbon materials. Structural ceramics like silicon carbide (SiC) combine a set of properties that make them excellent candidates for this application such as chemically inertness, low density, high thermal conductivity, excellent mechanical properties and low sinterability [7]. Furthermore, SiC is a semiconductor with a tunable bandgap depending on the doping that could exhibit electronic interaction with the metallic active phase of the catalyst [8,9]. In catalyst supports, a high surface area is usually sought (> $20 m^2/g$) to increase the dispersion of the active phase. SiC powder is usually prepared through the Acheson method [10] in which non-porous silica is reduced using carbon by passing an electrical current through the mixture. Due to the nature of the precursors and the synthesis process, the resulting SiC is inherently non-porous and presents a low surface area [11]. For these reasons, there is a need to develop methods to prepare SiC with a higher specific surface and a hierarchical porosity in the range of mesopores. So far, 4 different approaches have been used to obtain high-surface area SiC with hierarchical porosity: I) *Polymer derived ceramics*. This method utilizes polymers that contain Si and C in their chain and can form SiC through the pyrolysis of such polymer. With this method, SiC with a surface area of up to a 170 m^2/g have been obtained [12], II) *Gas-gas reactions*. This method is based on the nucleation of a solid phase in a gas mixture, using CH_4 as carbon precursor and SiH_4 as a silicon precursor. With this method SiC with a specific area up to 200 m^2/g has been synthesized [13,14] although the high surface area is a result of the small particle size (10-100 nm) rather than the presence of a pore system. The absence of porosity and the small particle size would make this kind of SiC unsuitable for powder bed reactor catalysis due to the associated high pressure drops, 3) *Gas-solid reaction*. This method utilizes carbon as a solid species and $SiCl_4$ as a gas species. This approach has yielded SiC with a specific area of around 30 m^2/g [15]. 4)

Alternatively to the latter method, a shape memory synthesis (SMS-SiC) was developed [16]. This technique utilizes activated carbon as the carbon source, with the aim of replicating the porous structure of the carbon precursor after conversion. To achieve this, the carbon is reacted with a silicon precursor (Si or SiO_2) obtaining a SiC with specific area up to 60 m^2/g.

The present work explores a novel approach where the concept is analogous to the aforementioned SMS-SiC but in which the precursor with a well-developed porosity is a mesoporous SiO_2. Chemical vapor deposition was used to introduce C (using a He:CH_4 mixture) within the pore system of the silica, followed by a thermal carboreduction to obtain mesoporous SiC. The use of a small hydrocarbon like CH_4 ensures the complete pore filling with C which acts as a stiff backbone to ensure a high degree of reproducibility of the original SiO_2 pore system. The obtained mesoporous SiC was characterized using N_2 gas adsorption and microscopy (FESEM, TEM). The filling mechanism of the pores within the precursor was studied using gas adsorption, thermogravimetric analysis (TGA-DTA) and SEM.

2. Experimental

2.1 Preparation of mesoporous SiO_2

Mesoporous silica (SiO_2) was prepared according to a sol-gel procedure described in detail elsewhere [17]. 0.400 g of Pluronic F127, a triblock copolymer surfactant terminating in primary hydroxyl groups (Sigma Aldrich, 99 % purity) and 0.452 g of Urea (Sigma Aldrich, 99.5% purity) were added to 5.052 g of acetic acid 0.01 M (Sigma Aldrich, 99.9 % purity). The mixture was stirred vigorously for 80 minutes. Then, the solution was introduced in an ice bath and 2.030 g of tetramethyl orthosilicate (TMOS, Sigma Aldrich, 98% purity) were added drop by drop. This solution was stirred for 40 minutes at 0 ^oC. Finally, the dissolution was introduced in a Teflon autoclave and was treated at 40 ^oC for 24 hours, followed by a hydrothermal treatment at 120 ^oC for 6 h. The final dry product was fired in air at 550 ^oC for 6 h using a heating ramp of 3 ^oC/min.

The final product (SiO_2) was characterized by means of gas adsorption (N_2 at -196 ºC) and field emission scanning electron microscopy (FESEM).

2.2 Chemical vapor deposition (CVD)

Carbon was deposited within the pores and on the surface of the SiO_2 using a chemical vapor deposition technique. For that purpose, 0.250 g of silica were introduced in a 5 mm diameter, U-shaped quartz reactor. The reactor was connected to a gas system (See Fig.1) that uses mass flow controllers to achieve accurate and homogeneous gas mixtures. With the goal of cleaning the surface of the silica, helium (He) was first flowed through the reactor with a flow rate of 50 ml/min for 30 min. After that, a CH_4/He (10:90 v/v)

mixture flowed through the reactor and the sample. Temperature in the reactor was increased to 925 ºC with a heating rate of 10 ºC/minute using a split-tube resistance furnace. To optimize the deposition process, different experiments were made with different dwell times at the target temperature (1,3,6 and 10 h).

The carbon/SiO_2 mixtures obtained were characterized by thermogravimetry, in oxidizing atmosphere (4:1 N_2:O_2) to determine the carbon content, and in inert atmosphere, to determine the beginning of the reaction between C and SiO_2. Physical gas adsorption (N_2 at -196 ºC) was used to analyze porosity evolution.

2.3 Reduction of SiO_2 to SiC

The SiO_2/C mixture was thermally treated under a flowing inert atmosphere (Ar) at 1450 ºC for 5 h to reduce the silica to SiC. After the reduction, the product was purified in two steps: 1) removal of residual C and 2) removal of unreacted SiO_2. To eliminate the residual carbon, the sample was placed in a crucible and thermally treated in oxidizing (open air) atmosphere at 800 ºC for 8 h, with a 10 ºC/min heating rate. The residual silica was eliminated by an acid treatment at 80 ºC for 24 hours using a mixture of concentrated hydrofluoric acid (HF, 40% v/v) and nitric acid (HNO3, 67% v/v) in a ratio of 9:1.

The pore structure and textural properties were evaluated using physical adsorption of gases (N_2 at -196 ºC), FESEM and TEM.

3. Results and discussion

3.1 Mesoporous silica (SiO_2)

Fig. 2a shows the N_2 adsorption isotherm of the starting silica. The material presents a type IVa isotherm according to the IUPAC classification [18], which is characteristic of mesoporous materials (pores ranging between 2-50 nm). The absence of an elbow in the isotherm at low relative pressures indicates a low concentration of micropores (pores < 2 nm). Fig. 2b shows the pore size distribution of the silica obtained using the Barret-Joyner-Halenda method (BJH). A broad pore size distribution in the range of 5-50 nm is observed. The pore size distribution falls completely in the mesoporous range, with the smaller porosity being closer to the microporous range (< 2 nm). There is no presence of macropores (pores > 50 nm) in the material.

The textural properties derived from the N_2 adsorption are shown in Table 1. The specific surface was calculated by applying the B.E.T. method and the micropore volume was estimated using the Dubinin-Raduskevich method. The mesopore volume is calculated as the difference the between total pore volume and micropores volume. The parameters D10, D50 (mean) and D90 represent the 10^{th}, 50^{th} and 90^{th} percentiles in the pore size distribution and were calculated from the accumulated volume curve.

The morphology of the silica is shown in Fig. 3. Silica particles present a spherical morphology with diameters that oscillate between 4 and 6 μm. Cazorla et al. propose that this morphology is a consequence of the combined effect of the spinodal decomposition and the solution/precipitation reaction of the silica that happens during the hydrothermal treatment at 120 ºC [17] .

3.2 Carbon deposition on silica

The selection of the C precursor is of key importance for the replication process. To replicate the porous structure of the precursor (SiO_2), the carbon precursor must be capable of spreading through the pore network and decompose to yield C that fills the pores. The deposited C can then act as a stiff backbone during the reduction of SiO_2 to guarantee that the precursor porous structure is maintained. Methane (CH_4) was selected as a precursor gas because the size of the molecule (0.3988 nm) is small enough to penetrate pores of the order of mesopores and even of the widest micropores and because methane has the slowest cracking rate among hydrocarbon to form pyrolytic carbon, therefore preventing early pore clogging that would hinder the pore filling. [19,20]. Methane decomposes on the surface of the silica (cracking reaction) according to the following reaction [21]:

$$CH_4(g) \rightarrow C(s) + 2H_2(g) \qquad (1)$$

The progress of the methane cracking reaction on the surface of the silica was monitored by using a mass spectrometer coupled to the reactor (Fig.4a) to analyze the evolution of the gases flowing out of the reactor. It was found that the temperature at which the uncatalyzed cracking begins is around 650 ºC as indicated by the formation of hydrogen gas. However, the reaction does not accelerate until above 900 ºC. This is consistent with a change in sign in the Gibbs free energy of the reaction (eq.2) which was calculated at different temperatures from the ΔG^0 [21] value, using the activity coefficient of the reaction ($Q = \frac{\left({p_{H2}}/{p_{H2,0}}\right)^2}{{p_{CH4}}/{p_{CH4,0}}}$), where p_0 is the partial pressure at a chosen reference state, in this case taken as 1 atm. We have assumed that at low pressures (atmospheric pressure) and for low reactivity gases in non-charged states like these, fugacity can be approximated as partial pressure. ΔG reaches a value of 0 at a temperature of 545 ºC and becomes negative at higher temperatures.[22]

$$\Delta G\left(\frac{J}{mol}\right) = 89{,}658.88 - 102.27T - 0.00428T^2 - \frac{2{,}499{,}358.99}{T} + RTlnQ \qquad (2)$$

For this reason, a temperature of 950ºC was used for all experiments to ensure maximum conversion of methane to carbon. Fig. 4b shows the evolution of methane (mass 16) and hydrogen (mass 2) over time at 950 ºC. There is a pronounced evolution of H_2 at the beginning of the isothermal period (1.5 h) that presents a maximum around 4h and then decreases slowing down after 8h. This hydrogen production is

accompanied by a methane consumption which suggests that the former is coming from the decomposition of methane thus ensuring that carbon is been deposited on the SiO_2.

To study the carbon deposition kinetics, experiments were performed with different holding times under isothermal conditions (1, 3, 6 and 10 h), and the deposit was evaluated on a gravimetric basis by TGA in oxidizing atmosphere. Fig. 5a and 5b show the N_2 adsorption isotherms for the different C/SiO_2 samples obtained with different isothermal holding times. Clearly, the shape of the isotherms is modified by the carbon deposition. The elbow observed at lower relative pressures becomes narrower for the samples subjected to a 1 and 3 h deposit, indicating increasing presence of narrow microporosity, and it disappears for the samples subjected to a 6 and 10 h deposit. The total adsorption capacity of the samples decreases gradually with the deposit time, which is consistent with the filling of the pores with carbon. As an exception, the sample subjected to a 1 h deposit has a slightly higher adsorption capacity than the precursor silica, most likely due to porous carbon deposit generated in the early stages. Fig. 5c shows a schematic representation of the proposed mechanism for pore filling. In early stages, namely 1-3 h of deposit, the carbon deposited on the silica pore walls decreases the pore size, turning the micropores into narrow micropores thus modifying the shape of the elbow at low relative pressures. As methane continues to decompose (6-10 h), the micropores become filled and the isotherms lose the characteristic elbow. On the larger porosity, gradual deposit on the pore wall causes a general pore diameter and pore volume decrease which decreases the total adsorption capacity of the material. Finally, after 10 h, most of the porosity has been filled with carbon.

Based on the weight measurements obtained from the TGA in air, the carbon content of each sample prepared at different deposit times was calculated. Fig. 6 shows this carbon content vs. deposit time. The amount of carbon deposited follows a sigmoid behavior with a plateau after 6 h. This behavior is well described by the Avrami model [23]. This model has been applied to several uncatalyzed gas-solid reactions [24–26] and proposes that the coverage of a surface (θ) where a gas product is reacting to yield a solid product on that surface is governed by

$$\theta = 1 - e^{-kt^n}$$

Where k is a constant that depends on the energy barrier necessary to form the nuclei and start growing and n is a parameter that determines the order of the equation and depends on how the nuclei grow. Table 2 illustrates the different possible mechanisms described by the model.

By assuming that after 10 h the covered of the surface is completed (θ = 1), the value of θ was estimated based on the C percentage determined by TGA. The Avrami equation was fitted to the experimental data and the best fit yielded a value of K=0.0757 and n=2.

Since graphite grows in layers, and the order of the equation was found to be n = 2, it would seem that at the beginning of the reaction, multiple graphitic nuclei form on the surface of the silica and continue to grow laterally to coalesce. The optimal time selected for carbon deposit was 6 hours, to ensure complete pore filling.

SEM images of the SiO_2-C sample after exposure to the He/CH_4 mixture for 6 h are shown in Fig. 7. A completely uniform deposit was observed throughout the silica. TEM images of the same sample are shown in Fig. 8. The carbon deposited exhibits a highly-ordered structure characterized by equidistant planes with a spacing equal to the interlayer spacing between graphene layers in graphite (d_{002}). The average thickness of the layer measured 8 nm.

3.3 Mesoporous Silicon carbide

A TGA in Ar atmosphere was carried out in the range of 25 ºC to 1500 ºC to determine the temperature at which the carboreduction of silica occurs. The obtained thermogram is shown in Fig. 9. The process of carboreduction begins around 1000 ºC. The differential of the TG signal (DTG) exhibits two distinct, more intense peaks (higher reaction rate), one around 1260 ºC and another 1350 ºC (the less intense peak around 1050 °C is assumed to be the start of the reactions associated with the peak observed at 1260 °C with a slower reaction rate and localized exclusively to the areas of immediate contact between SiO_2 and C). Weimer et. al. proposed that the reduction of silica occurs in steps described by the following chemical reactions [27]

$$C(s) + SiO_2(s) \rightarrow SiO(g) + CO(g) \quad (3)$$

$$C(s) + CO_2(g) \rightarrow 2CO(g) \quad (4)$$

$$CO(g) + SiO_2(s) \rightarrow SiO(g) + CO_2(g) \quad (5)$$

$$2C(s) + SiO(g) \rightarrow SiC(s) + CO(g) \quad (6)$$

The first DTG peak can be associated to reaction 3 and 6 occurring in series, corresponding to the formation of SiC where carbon is in contact with silica. Since both reactants are solids at the experimental conditions used once the contact points have been exhausted reaction 3 is slowed down and reactions 4 and 5 become rate-limiting. The SiO generated from reaction 5 diffuses through the porous SiC layer formed by reactions 3 and 6, and further conversion is achieved at higher temperature (second DTG peak). Yao et al.

determined that the carboreduction of silica is well described by a contracting volume shrinking core model with an irreversible phase boundary-controlled reaction of a sphere, where the reaction layer thickness is small compared to the size of the sphere. This model describes a thermally activated process that follows an Arrhenius behavior [28]. For this reason, to ensure maximum conversion, the carboreduction of the silica in this work was performed at 1450 °C.

After the carboreduction, the product was purified in 2 steps to remove residual SiO_2 or C (see Section 2.1). Residual precursors can have a huge impact on the surface area and mesoporous volume measurements and can lead to the wrong interpretation of the retention of the textural properties after conversion. To evaluate the complete removal of the precursors and that the product was solely comprised of SiC, TEM analysis was performed. Fig 10 shows a bright field TEM image of the SiC obtained with the corresponding lattice fringe. EDX analysis shows that the material is comprised of Si and C with a 1:1 ratio and some minimum amount of O probably picked up from the atmosphere.The distance between the crystalline planes measured corresponds to the spacing of 111 planes in SiC.

The textural properties of the synthesized SiC with hierarchical porosity were measured using gas adsorption. The N_2 adsorption isotherm of the silicon carbide obtained is shown in Fig.11. It corresponds to a type IV isotherm, according to the IUPAC classification [18] which is associated with mesoporous materials. The shape of the adsorption isotherm is evidence of a well-developed hierarchical pore system with pores in the range of mesopores. The adsorption isotherms reported for high-surface area SiC obtained with other methods are typically type II isotherms (associated with non-porous materials)[29]. SiC produced with larger hydrocarbon molecules such as propane [24], yield non-porous SiC with a type II isotherm. A high surface area is still achieved due to the small particle size of SiC. Large hydrocarbons cannot diffuse into the smallest porosity of the silica and hence no carbon is deposited within these pores. As a result, during the reduction step, these pores collapse and yield non-porous SiC particles thus achieving low retention of the silica textural properties. Methane, on the other hand, is a small molecule capable of diffusing into smaller mesoporosity and even into large microporosity (up to 0.39 nm).

The pore size distribution of the obtained SiC calculated with the BJH method is shown in Fig. 11. The largest population of pores is within 3-5 nm range. Similar to the original SiO_2 template, a broad distribution of pore sizes between 3 and 30 nm was also observed. Although the change in molar volume during the reaction is negative and should result in an increase in the average pore size (ΔV_m= - 44%), some authors have indicated that a low heating rate such as that used in this work may result in partial collapse of the microporous structures due to the lack of a rigid structure at the beginning of the reaction. Independently of the partial distortion, a high fraction of the starting pore network of the silica is retained in the synthesized SiC. The textural properties and pore size distribution of the SiC obtained are summarized

in Table 3. The volume of micropores was calculated by the Dubinin-Raduskevich method and the volume of mesopores was calculated by the difference between the total volume and micropores volume. This assumption could be made because there are hardly any macropores in this material as seen in Fig. 11b.

Even though the volume of mesopores in the obtained SiC is slightly lower than the mesopore volume of the starting silica, most likely due to the change in volume when forming SiC and/or the partial collapse of the mesoporous structures, the percentage of retention of the textural properties is significantly higher than the ones reported in literature so far. If we define the percentage of retention of a given property as:

$$R(\%) = \frac{X_{SiO_2} - X_{SiC}}{X_{SiO_2}}$$

Being X=S_{BET}, $V_{mesoporous.}$ With the synthesis method used in this work, 61% of the specific area (S_{BET}) and 47% volume of mesoporous are retained. The percentage retention of mesoporous volume using other synthesis methods such as the use of heavier hydrocarbons [29], or the case of using a liquid carbon precursor [28] is only 5 and 10% respectively. This lower retention of the textural features is most likely due to a steric effect where the precursors fail to fill the smaller porosity during the carbon impregnation. As a result, during the reduction step, there is no stiff support for the microstructure, causing the micro and mesoporous structures to colapse, thus losing mesoporous volume.

A FESEM image of this material is shown in Fig. 12. The overall spherical morphology of the original SiO_2 is retained. The surface roughness shows a significant increase due to the crystal morphology of SiC which exhibits faceted crystals. The size of the spheres has decreased from roughly 5 microns to approximately 1 micron, which is consistent with the molar volume decrease associated with the reduction of SiO_2 to SiC.

4. Conclusions

Mesoporous SiC with hierarchical porosity was successfully prepared by using a hard-templating method where mesoporous SiO_2 was used as template and CH_4 was used as the C precursor. From the optimization study of the C deposition it was concluded that the filling of the pores occurs gradually, first occluding microporosity and finally the mesopores. The optimal time for the C deposit by CH_4 cracking was 6 hours of isothermal hold at 950 ^oC with a gas stream comprised of 10% vol. CH_4 and 90% vol. He. The carboreduction of the prepared SiO_2-C material yielded SiC with a high content of mesopores and a wide pore size distribution. The retention of the specific surface and the mesopore volume from the template (SiO_2) were 61 and 47% respectively, 6-12 times higher than those reported so far in literature.

5. Acknowledgements

The authors would like to acknowledge the assistance of Dr. Jaime Garcia in preparing the mesoporous silica. Financial support from the Generalitat Valenciana under the PhD grant Vali+d and the "Ministerio de Economía y Competitividad" (Grant MAT2017-86992-R), and action Mobility of Alicante University is gratefully acknowledged.

6. References

1. Anderson JA, Fernández García M. Supported Metals in Catalysis. London: Im. 2005.
2. Schwarz JA, Contescu C, Contescu A. Methods for Preparation of Catalytic Materials. Chem Rev. 1995;95(3):477–510.
3. Yao HC, Stepien HK, Gandhi HS. Metal-support interaction in automotive exhaust catalysts: Rh-washcoat interaction. J Catal. 1980;61(2):547–50.
4. Munro RG. Material Properties of a Sintered SiC. Phys Chem. 1997;26(5):1195–203.
5. Keller N, Pham-huu C, Ledoux MJ, Estournes C, Ehret G. Preparation and characterization of SiC microtubes. 1999;187:255–68.
6. E. Levinshtein M, L. Rumyantsev S, S. Shur M. Properties of Advanced Semiconductor Materials: GaN, AIN, InN, BN, SiC, SiGe. Wiley & Sons J, editor. 2001. 93–104 p.
7. Acheson E. Production of Artificial Crystalline Carbonaceous Material. US; 492767, 1893.
8. Wei GC. Beta Sic Powders Produced by Carbothermic Reduction of Silica in a High-Temperature Rotary Furnace. J Am Ceram Soc [Internet]. 1983 Jul [cited 2017 May 24];66(7):c111–3. Available from: http://doi.wiley.com/10.1111/j.1151-2916.1983.tb10602.x
9. Chorley RW, Lednor PW. Synthetic routes to high surface area non-oxide materials. Adv Mater [Internet]. 1991 Oct [cited 2020 Apr 2];3(10):474–85. Available from: http://doi.wiley.com/10.1002/adma.19910031004
10. Ryan CE, Berman I, Marshall RC, Considine DP, Hawley JJ. Vapor-liquid-solid and melt growth of silicon carbide. J Cryst Growth [Internet]. 1967 Dec [cited 2017 Jul 26];1(5):255–62. Available from: http://linkinghub.elsevier.com/retrieve/pii/0022024867900310
11. Varshney SK, Beatty CL. Formation of Silicon Carbide and Silicon Nitride by Vapor-Phase Reaction. In: Proceedings of the 6th Annual Conference on Composites and Advanced Ceramic Materials: Ceramic Engineering and Science Proceedings. 1982.
12. Moene R, Makkee M, Moulijn J. High surface area silicon carbide as catalyst support

characterization and stability. Appl Catal A Gen [Internet]. 1998 Feb [cited 2017 Jul 26];167(2):321–30. Available from: http://linkinghub.elsevier.com/retrieve/pii/S0926860X97003268

13. Ledoux MJ, Pham-Huu C. High specific surface area carbides of silicon and transition metals for catalysis. Catal Today [Internet]. 1992 Jun 30 [cited 2019 Mar 22];15(2):263–84. Available from: https://www.sciencedirect.com/science/article/pii/092058619280179Q

14. García-Aguilar J, Miguel-García I, Berenguer-Murcia Á, Cazorla-Amorós D. Synthesis of Robust Hierarchical Silica Monoliths by Surface-Mediated Solution/Precipitation Reactions over Different Scales: Designing Capillary Microreactors for Environmental Applications. ACS Appl Mater Interfaces [Internet]. 2014 Dec 24;6(24):22506–18. Available from: http://dx.doi.org/10.1021/am506595c

15. Thommes M, Kaneko K, Neimark A V., Olivier JP, Rodriguez-Reinoso F, Rouquerol J, et al. Physisorption of gases, with special reference to the evaluation of surface area and pore size distribution (IUPAC Technical Report). Pure Appl Chem. 2015;87(9–10):1051–69.

16. Becker A, Hüttinger KJ. Chemistry and kinetics of chemical vapor deposition of pyrocarbon - IV pyrocarbon deposition from methane in the low temperature regime. Carbon N Y. 1998 Jan 1;36(3):213–24.

17. Vignoles GL, Langlais F, Descamps C, Mouchon A, Le Poche H, Reuge N, et al. CVD and CVI of pyrocarbon from various precursors. Surf Coatings Technol. 2004 Nov 1;188–189(1-3 SPEC.ISS.):241–9.

18. Villacampa JI, Royo C, Romeo E, Montoya JA, Del Angel P, Monzón A. Catalytic decomposition of methane over Ni-Al2O3 coprecipitated catalysts. Appl Catal A Gen [Internet]. 2003 Oct [cited 2019 Oct 1];252(2):363–83. Available from: https://linkinghub.elsevier.com/retrieve/pii/S0926860X03004927

19. Amin AM, Croiset E, Epling W. Review of methane catalytic cracking for hydrogen production. Int J Hydrogen Energy [Internet]. 2011 Feb [cited 2019 Oct 2];36(4):2904–35. Available from: https://linkinghub.elsevier.com/retrieve/pii/S0360319910022500

20. Avrami M. Kinetics of phase change. II Transformation-time relations for random distribution of nuclei. J Chem Phys. 1940;8(2):212–24.

21. Tomellini M. Coverage-time dependence during island growth at a solid surface with application to diamond deposition from the gas phase. J Appl Phys. 1992;72(4):1589–94.

22. V. Sotirchos S. On a class of random pore and grain models for gas-solid reactions. Chem Eng Sci. 1987;42(5):1262–5.

23. Ballal G, Zygourakis K. Evolution of Pore Surface Area during Noncatalytic Gas-Solid Reactions. 1. Model Development. Am Chem Soc. 1987;26(5):911–21.

24. W. Weimer A, J. Nilsen K, A. Cochran G, P. Roach R. Kinetics of Carbothermal Reduction Synthesis of Betta Silicon Carbide. Ceram Adv Mater. 1993;39(3).

25. Yao J, Wang H, Zhang X, Zhu W, Wei J, Cheng YB. Role of pores in the carbothermal reduction of carbon-silica nanocomposites into silicon carbide nanostructures. J Phys Chem C. 2007;111(2):636–41.

26. Parmentier J, Patarin J, Dentzer J, Vix-Guterl C. Formation of SiC via carbothermal reduction of a carbon-containing mesoporous MCM-48 silica phase: A new route to produce high surface area SiC. Ceram Int. 2002;28(1):1–7.

FIGURE CAPTIONS

Figure 1. Schematic representation of the setup used to perform the chemical vapor deposition experiments.

Figure 2. (a) N_2 adsorption isotherm at-196 °C of the synthesized silica, and (b) pore size distribution calculated with the BJH method.

Figure 3. Secondary electron SEM images of mesoporous SiO_2 particles at different magnifications. Reprinted with permission from ACS Appl. Mater. Interfaces 2014, 6, 24, 22506-22518. Copyright (2014) American Chemical Society.

Figure 4. (a) CH_4 and H_2 evolution vs. temperature derived from the mass spectrometer results and ΔG of the reaction. (b) evolution of CH_4 and H_2 vs. time under isothermal conductions derived from the mass spectrophotometer results.

Figure 5 (a) Adsorption isotherm of silica deposited with carbon, (b) isotherm at low pressures and (c) scheme of micropores and mesoporous filing on the silica.

Figure 6. Carbon content and surface coverage (θ) vs. deposit time at 925 ˚C.

Figure 7. SEM images from SiO_2-C material at different magnifications.

Figure 8. TEM images of a SiO_2-C obtained after 6 h of carbon deposit at different magnifications.

Figure 9. TGA in Ar atmosphere of SiO_2-C.

Figure 10. TEM images of mesoporous silicon carbide at different magnifications, along with its composition estimated using EDX.

Figure 11. (a) Adsorption Isotherm of N_2 at -196 °C of SiC and (b) pore size distribution of SiC calculated by the BJH method

Figure 12. FESEM images of mesoporous silicon carbide at different magnifications.

TABLE CAPTIONS

Table 1. Textural properties of the silica.

Table 2. Different possible mechanism described by the Avrami model.

Table 3. Textural properties and pore size distribution parameters for the mesoporous SiC obtained and the starting SiO_2.

SiO_2					
S_{BET} (m^2/g)	$V_{micropores}$ (cm^3/g)	$V_{mesopores}$(cm^3/g)	D10 (nm)	D50(nm)	D90(nm)
193	0.07	0.64	8.7	16.3	23.4

	One-dimensional growth (like needles)	Two-dimensional growth (flat sheets)	Three-dimensional growth (spheres)
All nuclei are present at the beginning	n=1	n=2	n=3
The nuclei form at stationary speed	n=2	n=3	n=4

	$S_{BET\ (}m^2/g)$	$V_{micropores}(cm^3/g)$	$V_{mesopores}(cm^3/g)$	D10 (nm)	D50 (nm)	D90 (nm)
SiO_2	193	0.07	0.64	8.7	16.3	23.4
SiC	118	0.03	0.30	3.6	7.3	28.4

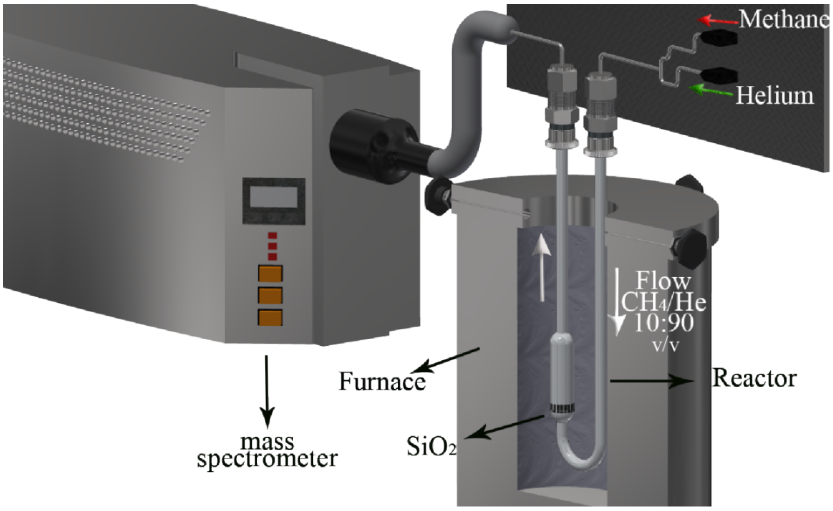

jace_17285_f1.png

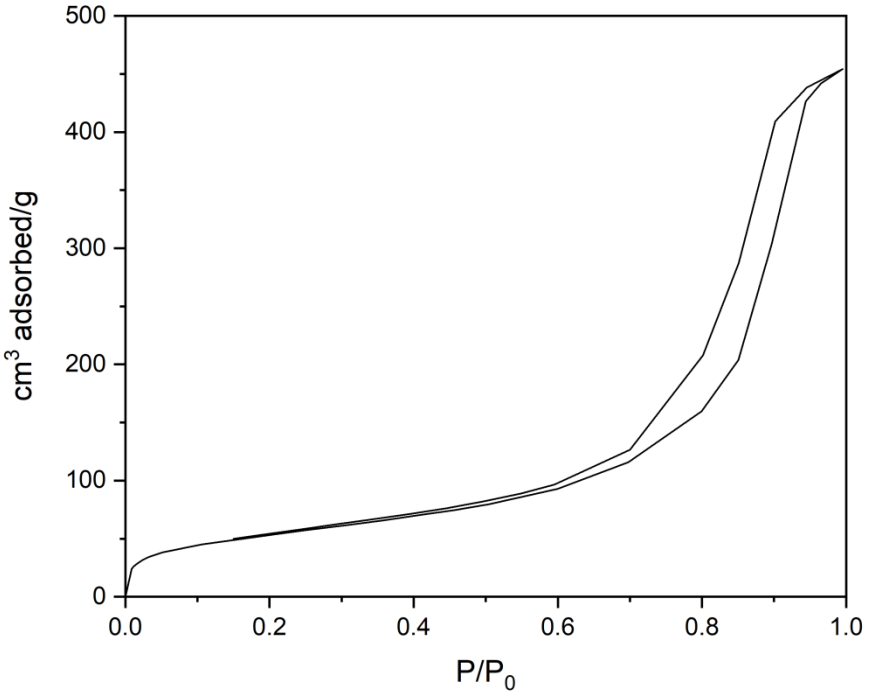

jace_17285_f2a.png

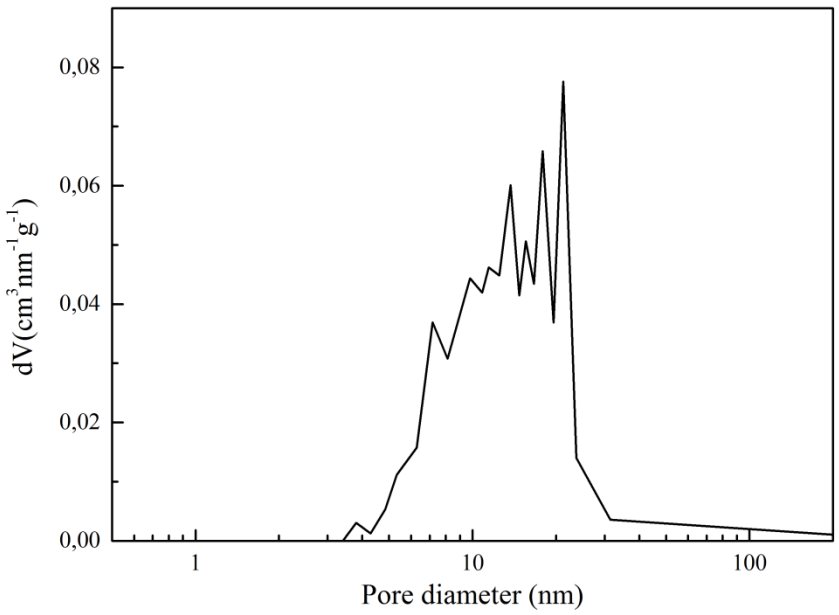

jace_17285_f2b.png

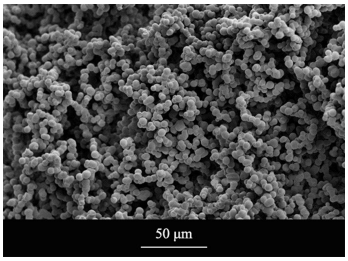

jace_17285_f3a.png

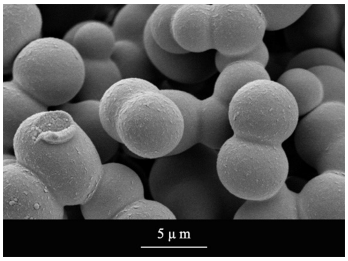

jace_17285_f3b.png

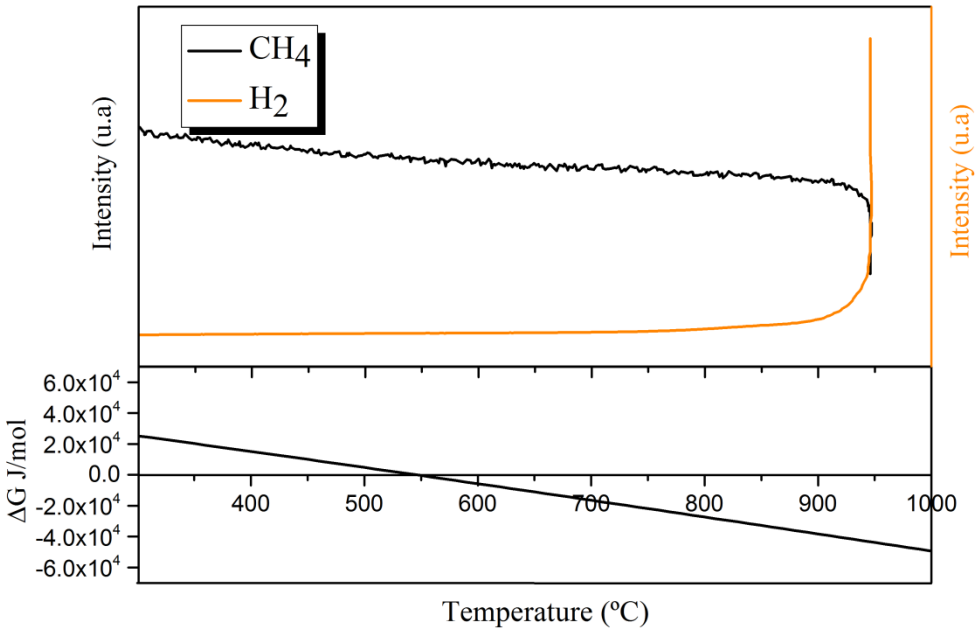

jace_17285_f4a.tif

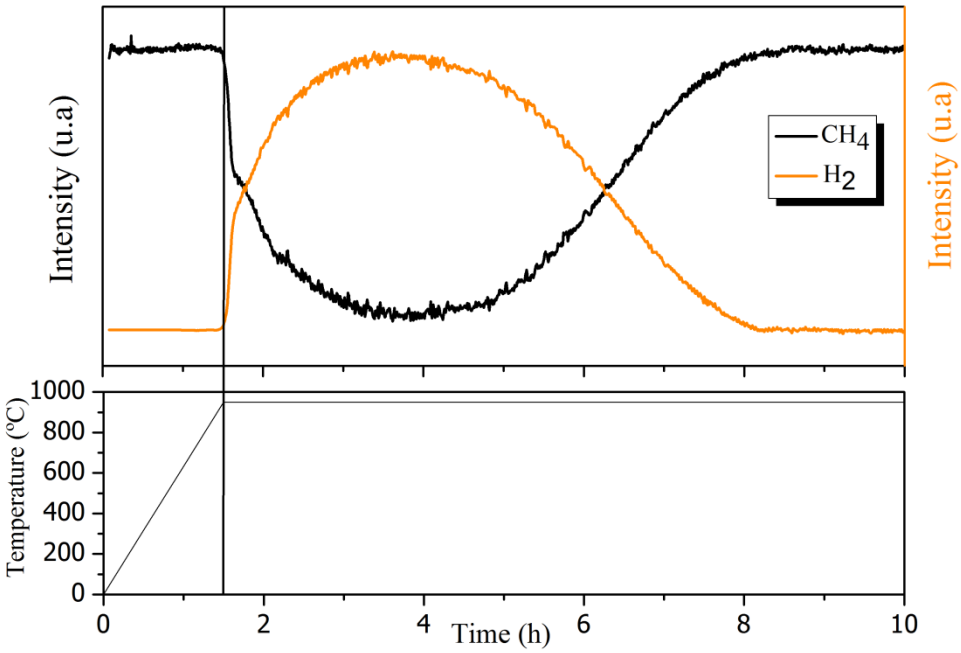

jace_17285_f4b.tif

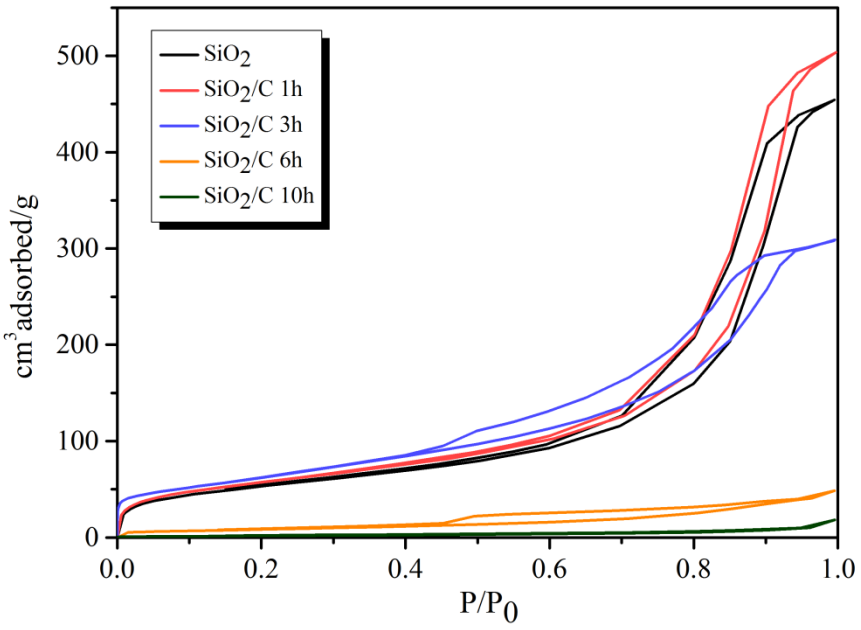

jace_17285_f5a.tif

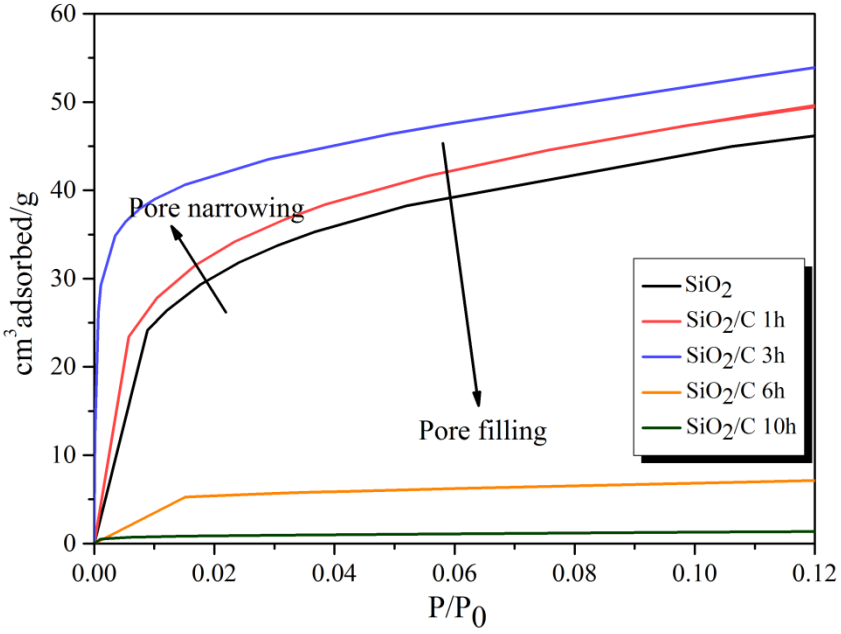

jace_17285_f5b.tif

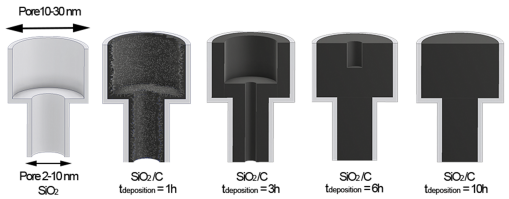

jace_17285_f5c.png

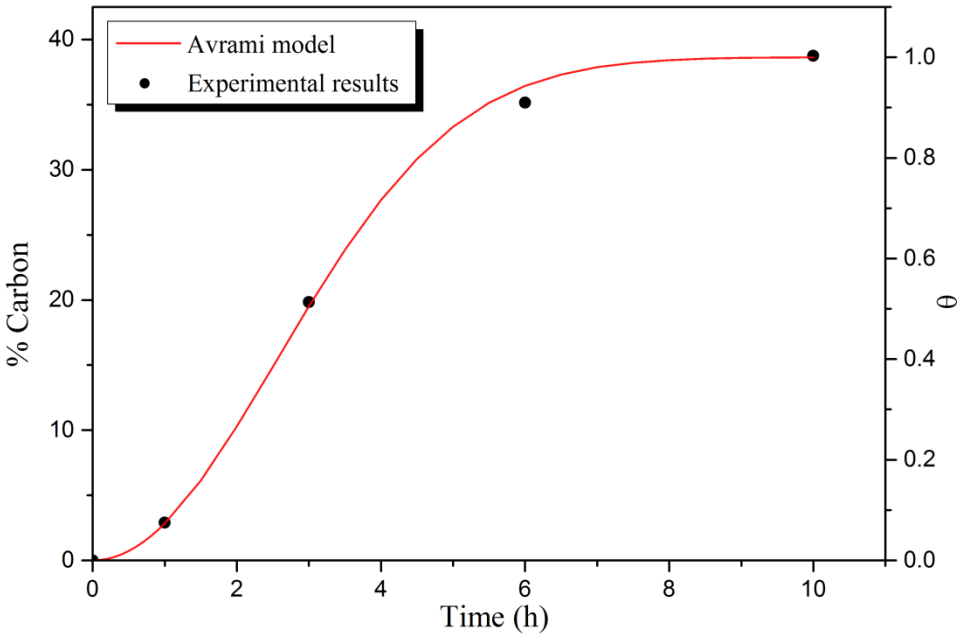

jace_17285_f6.tif

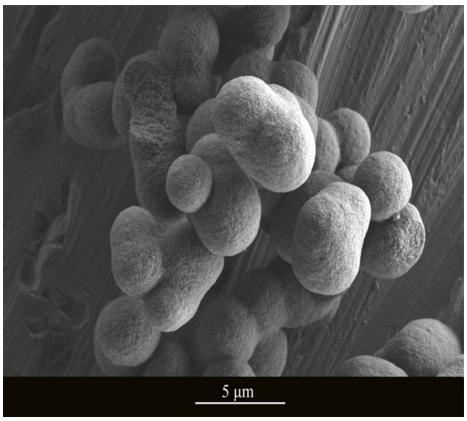

jace_17285_f7a.png

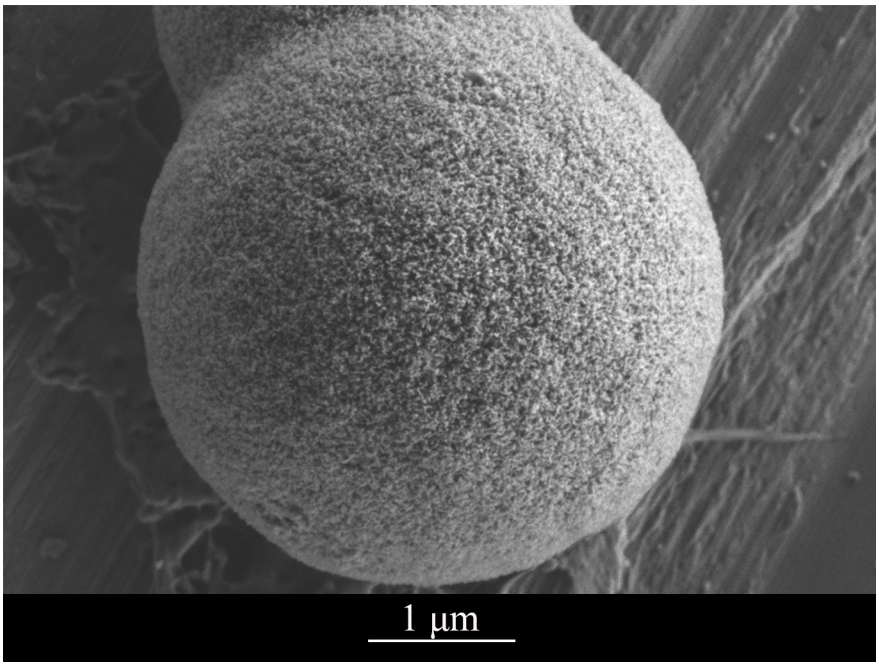

jace_17285_f7b.png

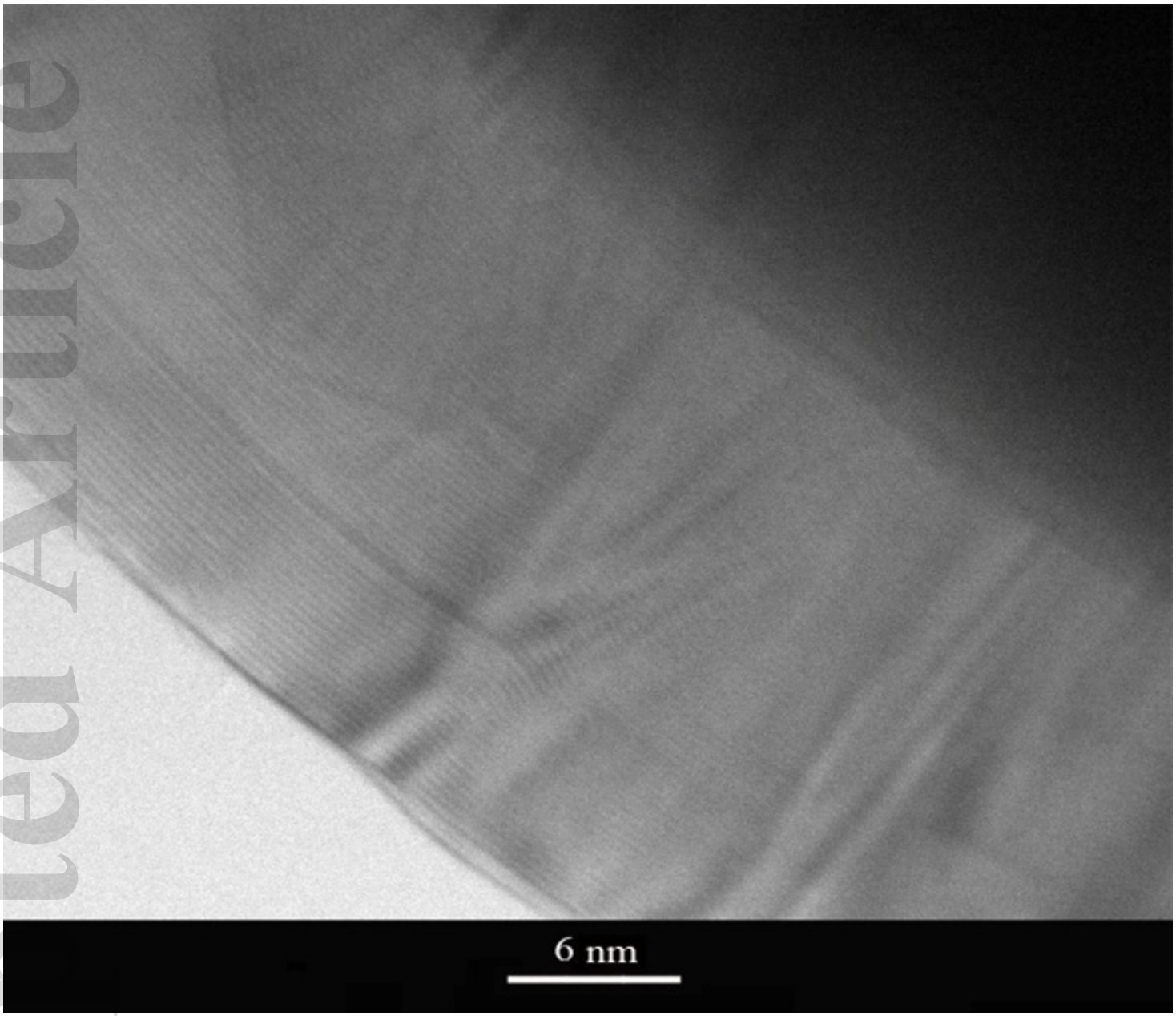

jace_17285_f8a.jpg

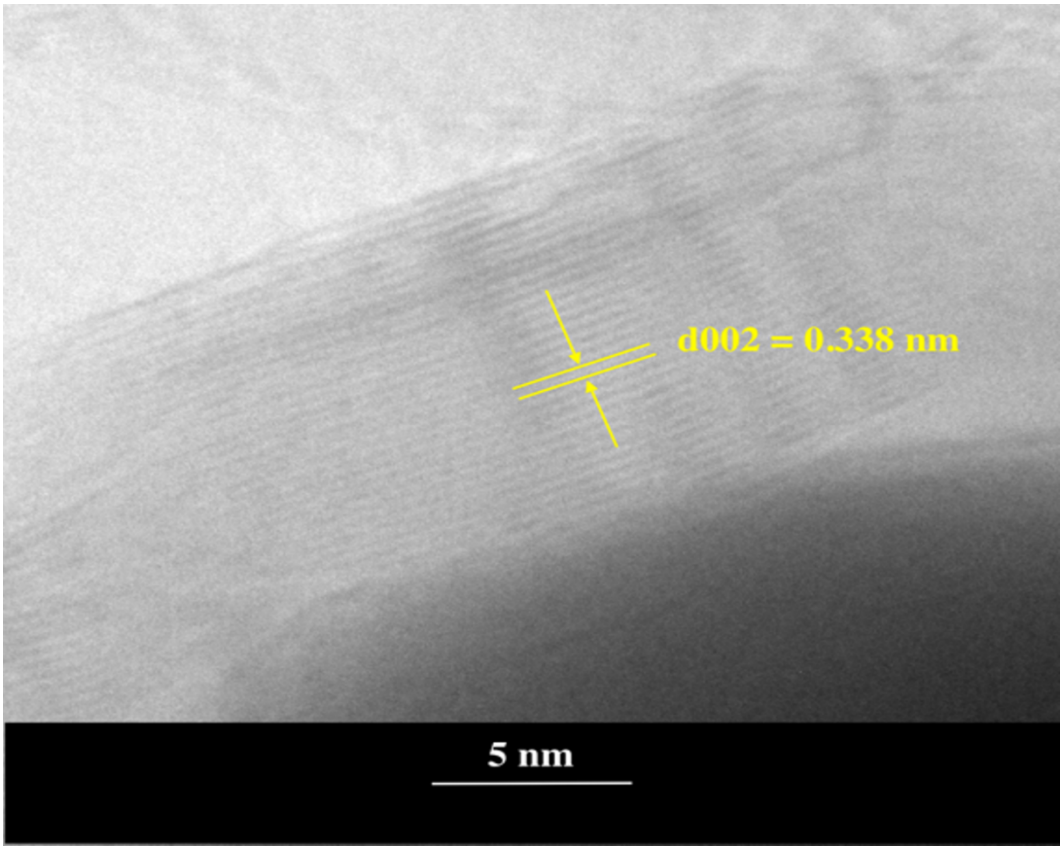

jace_17285_f8b.tif

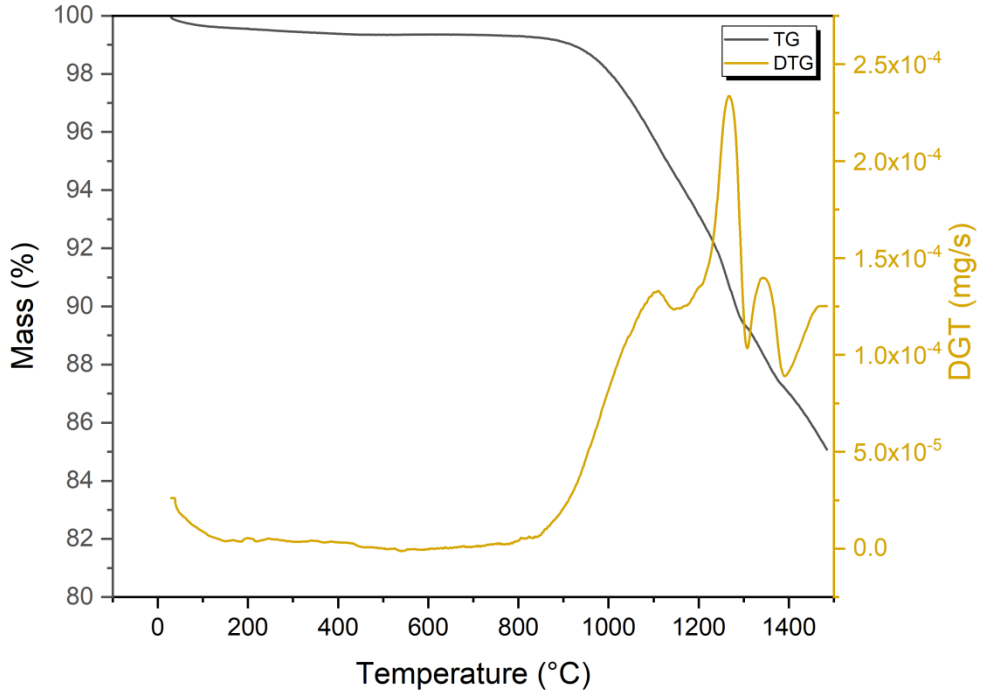

jace_17285_f9.png

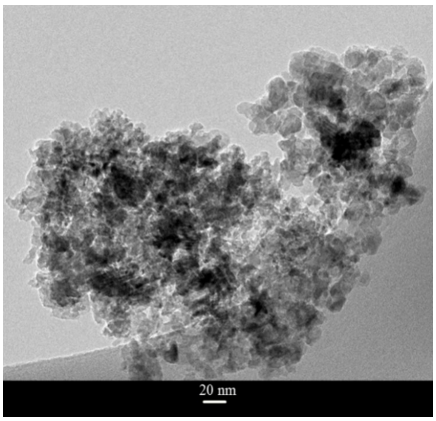

jace_17285_f10a.png

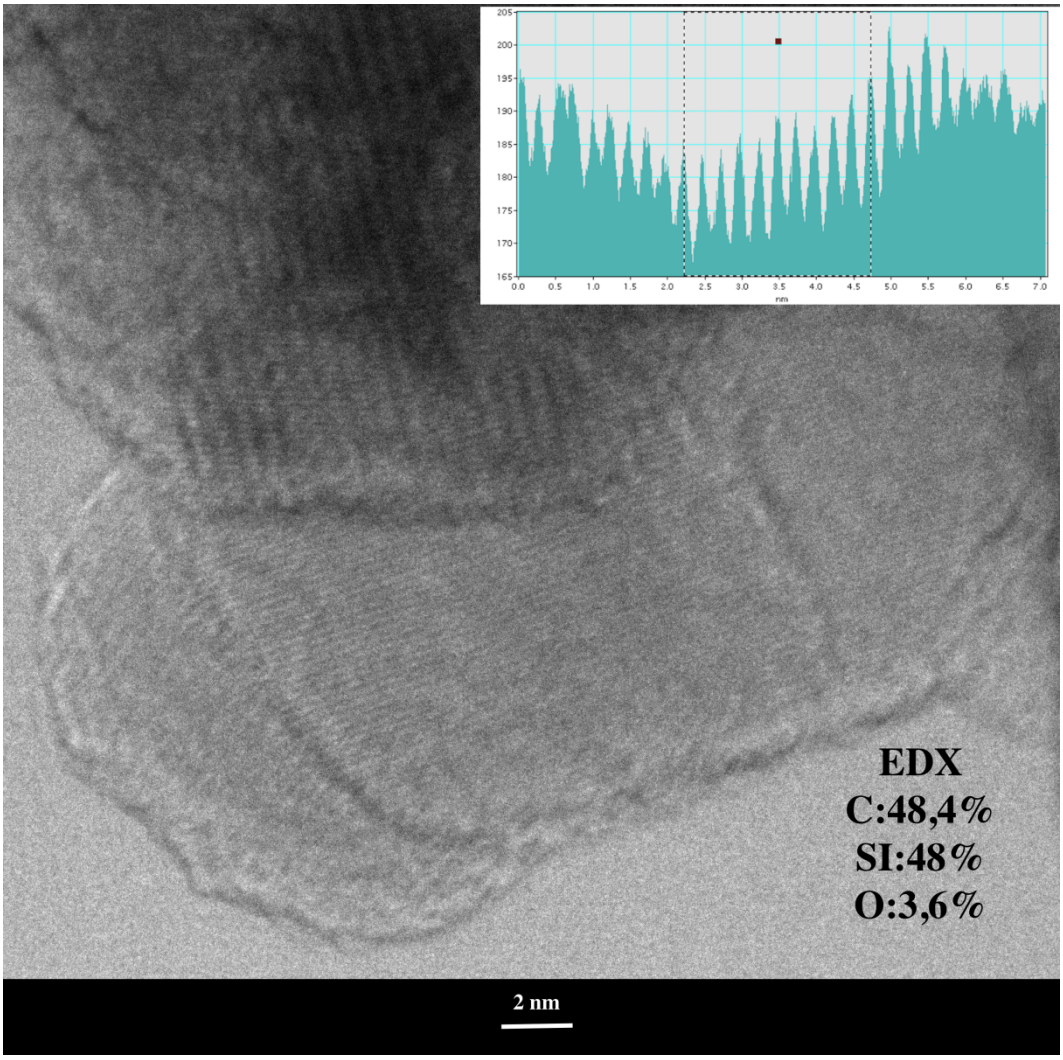

jace_17285_f10b.tif

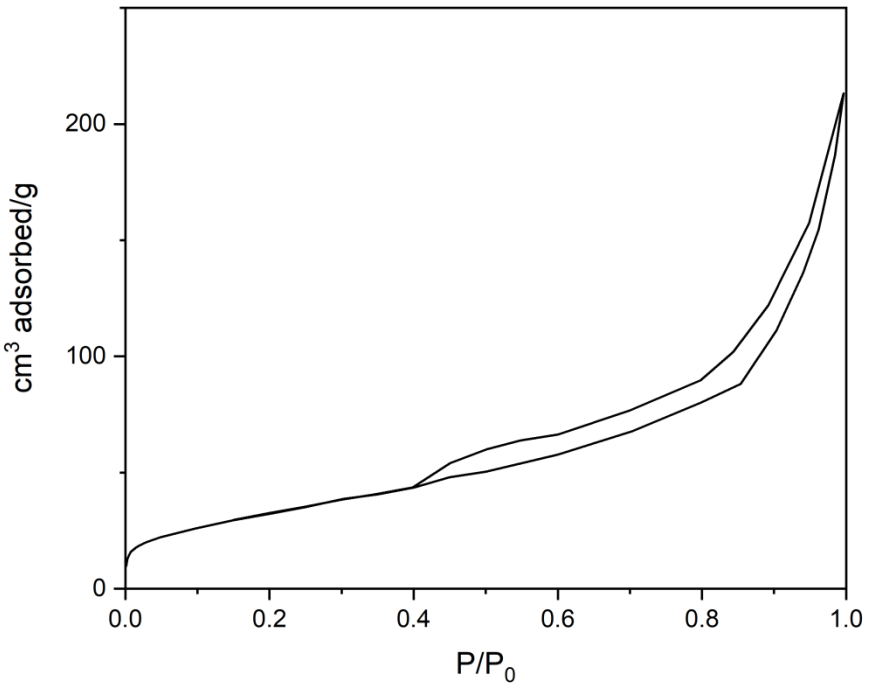

jace_17285_f11a.png

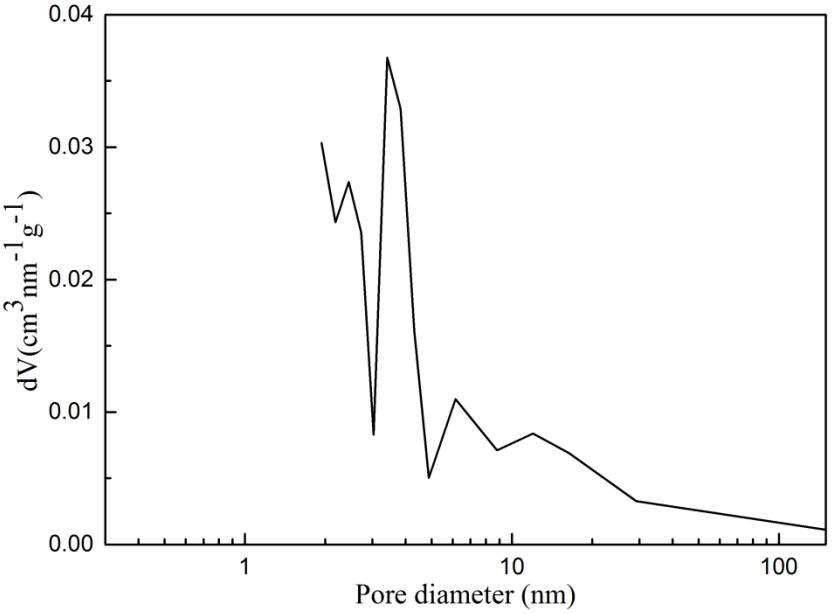

jace_17285_f11b.tif

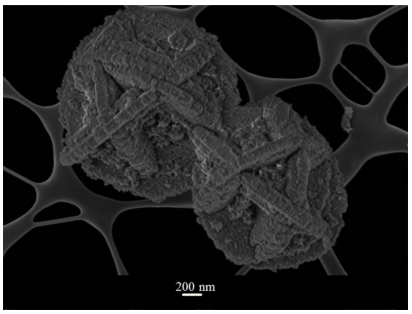

jace_17285_f12a.png

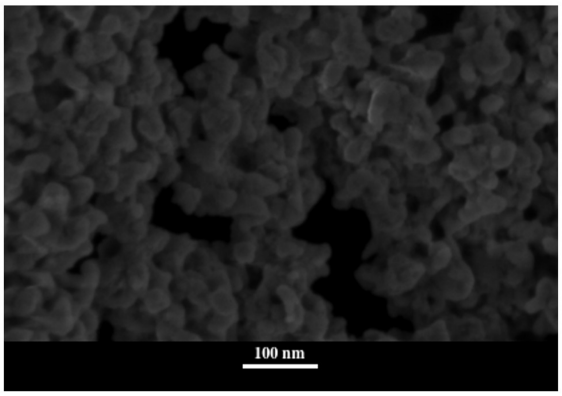

jace_17285_f12b.png